Article:
Esmaeili, M, Motagh, M and Hooper, A (2017) Application of Dual-Polarimetry SAR Images in Multitemporal InSAR Processing. IEEE Geoscience and Remote Sensing Letters, 14 (9). pp. 1489-1493. ISSN: 1545-598X

https://doi.org/10.1109/LGRS.2017.2717846

Application of Dual-Polarimetry SAR Images in Multi-Temporal InSAR Processing

Mostafa Esmaeili, Mahdi Motagh and Andy Hooper

Abstract **Multi-temporal polarimetric Synthetic Aperture Radar (SAR) data can be used to estimate the dominant scattering mechanism of targets in a stack of SAR data and improve the performance of SAR interferometric methods for deformation studies. In this paper we developed a polarimetric form of amplitude difference dispersion (ADD) criterion for time-series analysis of pixels in which interferometric noise shows negligible decorrelation in time and space in small baseline algorithm. The polarimetric form of ADD is then optimized in order to find the optimum scattering mechanism of the pixels, which in turn is used to produce new interferograms with better quality than single-pol SAR interferograms. The selected candidates are then combined with temporal coherency criterion for final phase stability analysis in full-resolution interferograms. Our experimental results derived from a dataset of 17 dual polarization X-band SAR images (HH/VV) acquired by TerraSAR-X shows that using optimum scattering mechanism in the small baseline method improves the number of pixel candidates for deformation analysis by about 2.5 times in comparison to the results obtained from single-channel SAR data. The number of final pixels increases by about 1.5 times in comparison to HH and VV in small baseline analysis. Comparison between Persistent Scatterer (PS) and small baseline methods shows that with regards to the number of pixels with optimum scattering mechanism, the small baseline algorithm detects 10 percent more pixels than PS in agricultural regions. In urban regions, however, the PS method identifies nearly 8 percent more coherent pixels than small baseline approach.**

Index Terms—**Polarimetric optimization, Slowly-Decorrelating Filtered Phase, Amplitude Difference Dispersion, Tehran plain**

I. Introduction

INTERFEROMETRIC analysis of Synthetic Aperture Radar (SAR) data is a powerful geodetic technique to measure surface deformations [1]–[4]. The accuracy achieved with interferometric measurements depends on a variety of factors including temporal and geometrical decorrelation, variations in atmospheric water vapor between SAR data acquisitions and the accuracy of orbital and Digital Elevation Model (DEM) used in the processing [5]. In order to address these limitations, multi-temporal InSAR time-series processing techniques such as small baseline algorithms and Persistent Scatterer InSAR (PSI) have been developed. The main goal of these techniques is to identify pixels for which the effect of the interferometric noise is small, so that they remain stable over the whole period of SAR data acquisition [6]–[8].

The PSI technique, firstly proposed by [6], [7], presents a solution to deal with spatiotemporal decorrelations of interferometric phase using time-series analysis of single-master interferograms. The technique uses Amplitude Dispersion Index (ADI) as a proxy of phase stability to identify pixels whose scattering properties are coherent between SAR image acquisition with long time interval and different look angles, the so-called Permanent Scatterer (PS). As interferograms are generated with a common master, PSs are limited to those pixels that show high coherence even in interferograms with larger baselines than the critical baseline [6], [7]. In [8] a new PS technique was proposed in which both amplitude and phase criteria are assessed to determine the stability of PSs. An initial set of candidate pixel based on amplitude analysis is selected first and then in an iterative process the PS probability is refined using phase analysis. The method is more suitable for detecting low-amplitude PS pixels in natural terrains, where the relationship between ADI index and phase stability breaks down.

Small baseline techniques use interferograms with small temporal and spatial baselines to reduce decorrelation. The original small baseline technique [9] uses a network of multi-looked small baseline interferograms and the target scatterers are identified by coherence (i.e. complex correlation) criterion [10], [11]. The multi-looking is a limiting factor for detecting local deformations. This issue was resolved in [12] with an extended version of small baseline algorithm applied on full-resolution SAR dataset. *Hooper (2008)* proposed another new small baseline method in which full-resolution differential interferograms are used to identify stable scatterers incorporating both amplitude and phase criterion. The filtered phase of those pixels that decorrelate little over short time intervals of interferograms, the so-called Slowly-Decorrelating Filtered Phase (SDFP) pixels are then used for deformation analysis [13].

Polarimetric optimization of polarimetric SAR data has been applied to improve classical InSAR results [14], [15] in terms of both deformation estimation and target classification [16], [17]. Optimization can be applied to full polarimetric space-borne SAR data [18], [19], ground-based fully PolSAR acquisitions [20] or compact polarimetric SAR data [21]–[23] The approach improves results by finding the scattering mechanism that minimizes decorrelation for each pixel over time, using coherence stability criteria or ADI, thereby maximizing the quality and number of selected PS pixels [17],

M. Esmaeili is with School of Surveying and Geospatial Engineering, College of Engineering, University of Tehran, Tehran, Iran (E-mail: maesmaeili@ut.ac.ir).

M. Motagh is with GFZ German Research Center for Geosciences, Department of Geodesy, Remote Sensing Section, 14473 Potsdam, and also with institute for Photogrammetry and GeoInformation, Leibniz Universität Hannover, 30167 Hannover, Germany (E-mail: Motagh@gfz.potsdam.de)

A. Hooper is with COMET, School of Earth and Environment, University of Leeds, Leeds, LS2 9JT, UK (E-mail: a.hooper@leeds.ac.uk).

[22], [24]–[26].

In this study, for the first time, we have developed a polarimetric optimization approach based on the small baseline method of the Stanford Method for Persistent Scatterers and Multi-Temporal InSAR (StaMPS/MTI) analysis presented in [13]. In our algorithm, instead of applying ADI criterion, we utilize Simulated Annealing (SA) optimization to minimize the Amplitude Difference Dispersion (ADD) value of each pixel. This can be employed as a rough proxy for phase variance for Gaussian scatterer pixels and it is an indicator for potential of a pixel to be a SDFP candidate, in dual polarimetry X-band SAR images, followed by projection of the polarimetric interferograms onto the optimized polarimetric channel to reproduce the interferograms with the optimum scattering mechanism. As proposed in [17], SDFP candidates are selected based on lower values of ADD in reproduced interferograms. In an additional step, the phase stability of each candidate is tested using a measure similar to coherence magnitude called temporal coherence [8], [13] and SDFP pixels are extracted. Time-series analysis and 3-D phase unwrapping are then carried out to retrieve the deformation parameters. We evaluate the method with a dataset consisting of 17 dual polarization X-band SAR data (HH/VV) acquired by TerraSAR-X satellite between July 2013 and January 2014 over Tehran plain, Iran (Fig. 1).

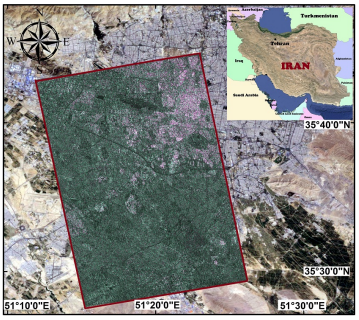

Fig. 1. RGB composite of study area produced by amplitude of dual-pol TerraSAR-SX images over Tehran plain (R=HH channel, G= VV channel and B=HH-VV channel) overlaid on Google-Earth image.

II. PIXEL SELECTION IN MULTI-TEMPORAL INSAR

In the StaMPS small baseline method, a set of candidate pixels for time-series analysis are first selected based on the amplitudes of SAR interferograms, to reduce the computational cost time. An index called ADD has been presented ($D_{\Delta A}$) to identify SDFP candidates [13].

$$D_{\Delta A}=\frac{\sigma_{\Delta a}}{\bar{a}}=\frac{\sqrt{\sum_{i=1}^{N}\left(\Delta A_i-\overline{\Delta A}\right)^2/N}}{\sum_{i=1}^{N}\left(|M_i|+|S_i|\right)/2N},\ \Delta A_i=|M_i|-|S_i| \qquad (1)$$

Where $\sigma_{\Delta a}$ is the standard deviation of the difference in amplitude between master and slave images, ΔA is the difference in amplitude between master and slave images, $\bar{a}$ is the mean amplitude and N is the number of interferograms. In this method a higher value of ADD in comparison with ADI, e.g. 0.6, is selected for the threshold and pixels with ADD value less than the threshold are considered as SFDP candidates. The residual phase noise for SDFP candidates is estimated by subtracting two major components of signal: spatially correlated and spatially uncorrelated components. Finally SDFP pixels are identified among the candidates using temporal coherence [8], [13], defined as:

$$\gamma_x=\frac{1}{N}\left|\sum_{i=1}^{N}\exp\{j(\varphi_{x,i}-\hat{\varphi}_{x,i}-\Delta\hat{\varphi}^{u}_{\theta,x,i})\}\right| \qquad (2)$$

Where $\varphi_{x,i}$ is the wrapped phase of pixel x in the ith interferograms, $\hat{\varphi}_{x,i}$ is the estimate for the spatially-correlated terms, $\Delta\hat{\varphi}^{u}_{\theta,x,i}$ is the estimate of the spatially-uncorrelated look angle error term and N is the number of interferograms.

For dual-pol SAR data we need to extend the ADD in (1), which is applicable only for single-pol data, to include also dual-pol data and optimize it to increase the density of SDFP pixels for the time-series analysis. We then apply temporal coherence in (2) to identify the SDFP pixels.

Fig. 2 shows a flow chart of the overall processing strategy that is implemented in this study. The method consists of 3 main steps: (1) InSAR processing, (2) polarimetric optimization and (3) multi-temporal analysis of the optimized interferograms. Single-pol multi-temporal InSAR analysis includes only InSAR processing (step 1) and time-series analysis of the interferograms (step 3). Polarimetric optimization is used here to improve the performance of this analysis using dual-pol data. In the next section we describe in detail the methodology we used in our study.

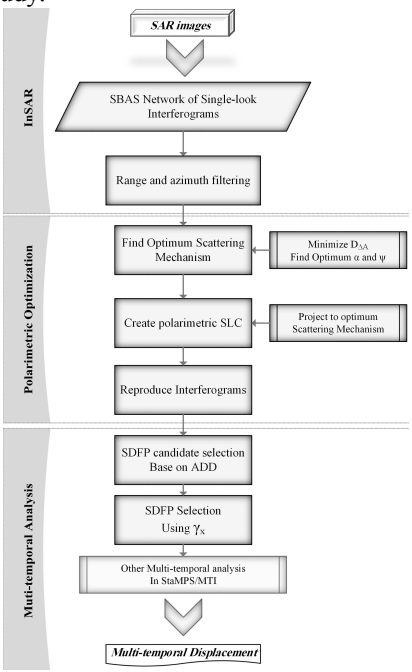

Fig. 2. Flowchart of the overall process in our study.

III. ADD OPTIMIZATION

In order to obtain the polarimetric form of ADD it is sufficient to replace the amplitude of single-pol data in **Error! Reference source not found.** by the polarimetric scattering coefficient, μ defined as:

$$\mu=\omega^{*T}\,\underline{K} \qquad (3)$$

$$\underline{K}=\frac{1}{\sqrt{2}}\left[S_{hh}+S_{vv},S_{hh}-S_{vv}\right]^T \qquad (4)$$

$$\underline{\omega}=[\cos(\alpha)\ \sin(\alpha)e^{j\psi}]^T,\qquad 0\le\alpha\le\pi/2,-\pi\le\psi\le\pi \qquad (5)$$

Where K stands for the polarimetric vector, ω is the

polarimetric projection vector, S_{vv} and S_{hh} are the complex values of the HH and VV channels, respectively, T is the transpose operator and * denotes the conjugate operator. α and ψ are Pauli parameters which represent the scattering mechanism [17], [22], [27]. The polarimetric form of ADD in (1) can then be written in the following form:

$$D_{\Delta A}^{Pol}=\frac{\sqrt{\sum_{i=1}^{N}\left(\Delta A_i^{Pol}-\overline{\Delta A^{Pol}}\right)^2/N}}{\sum_{i=1}^{N}\left(\left|\omega^{*T}K_i^M\right|+\left|\omega^{*T}K_i^s\right|\right)/2N},\quad \Delta A^{Pol}=\left|\omega^{*T}K^M\right|-\left|\omega^{*T}K^S\right| \tag{6}$$

Where $\underline{K}_i^M$ and $\underline{K}_i^S$ are polarimetric vectors of master and slave images, respectively.

The main objective of polarimetric optimization is to find the optimum scattering mechanism of the pixels and generate interferograms with better quality than using single-pol SAR images. To simplify the search of the optimum scattering mechanism, we parameterized the projection vector, in terms of Pauli basis parameters. In order to build consistent time series of phases related to deformation we assume that the scattering mechanisms of the pixels remain the same during acquisition time, as in the case of Multi-Baseline Equal Scattering Mechanism (MB-ESM). Therefore, ω would be the same for the pixel in whole stack of interferograms [28].

The optimization problem is to find the projection vector that minimizes the value of ADD. Fig. 3 illustrates the possible ADD values, in terms of α and ψ, for three arbitrarily selected pixels in our study area. In [17] we showed that SA is an effective method to minimize such smooth functions as illustrated in Fig. 3 and to find the optimum α and ψ in their corresponding finite range. We define a coarse grid with a step size of 10˚ for both α and ψ and search for the values that give the minimum ADD. These values for α and ψ are then used as initial values in the SA optimization method.

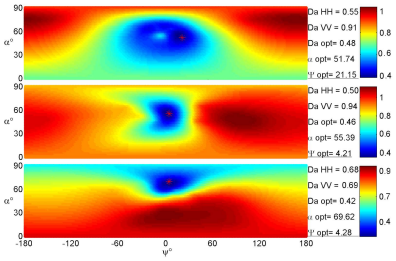

Fig. 3. Values of ADD for all possible values for α and ψ, for three arbitrarily selected pixels. The red star presents the minimum value of ADD.

IV. Experimental Results and Discussion

To evaluate the method we processed 17 co-polar SAR images acquired by TerraSAR-X satellite in an ascending mode between July 2013 and January 2014 over the Tehran plain, which is highly affected by subsidence [29]. We formed a small baseline network consisting of 44 single-look interferograms as shown in fig. 4. We then generated interferograms for HH, VV and optimum channels and calculated the ADD value of each pixel in the single-look interferograms. To evaluate the improvement in ADD, we compared the histograms of ADD values for HH, VV and optimum channel (Fig. 5).

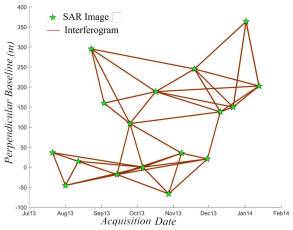

Fig. 4. Small baselines network used in this study. The stars denotes the SAR images and lines present the formed interferograms for Small Baseline processing.

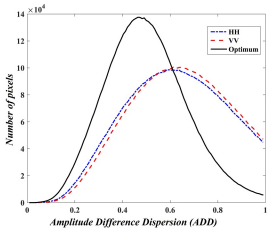

Fig. 5. Histograms of ADD for HH, VV and optimum channel.

As shown in Fig. 5, by applying the proposed method, the histogram of ADD values in optimum channel is inclined to lower values of ADD in comparison to HH and VV channels. Therefore, by thresholding ADD value of less than 0.6, more SDFP candidates are extracted in optimum channel as compared to single-pole interferograms.

Fig. 6 depicts the number of selected SDFP candidates obtained from HH, VV and optimum channels using ADD criterion and also the improvement in number of SDFP pixels after utilizing temporal coherency.

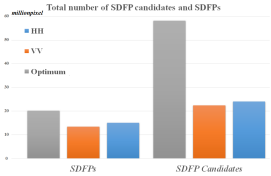

Fig. 6. Number of SDFP Candidates and SDFP pixels obtained by HH, VV and optimum channel.

The total number of SDFP candidates for the optimum channel is about 2.5 times higher than for the HH and VV channels. Considering the final selection of SDFP pixels for the optimum channel, the number has increased by about 1.4 times and 1.6 times in comparison to the HH and VV channels, respectively.

In order to evaluate the efficiency of using multi-temporal polarimetric SAR data for different models of scattering we made a comparison between urban and non-urban regions. 46 percent of our study area comprises urban region, while the non-urban portion is about 54 percent. In urban areas, the number of identified candidates using the optimum channel is increased by ~1.7 and ~2.1 times compared to HH and VV channels, respectively. For agricultural regions, the increase was ~2.1 and ~2.2 times (fig. 7b). The number of final SDFP pixels are ~1.4 and ~1.5 times in urban regions and ~1.48 and ~1.65 times in agricultural regions, in comparison to HH and VV channels, respectively (fig. 7a). Therefore the proposed algorithm is slightly more successful in non-urban regions than in urban regions.

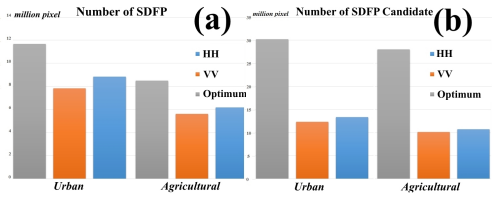

Fig. 7. Number of a) identified SDFP pixels and b) SDFP candidates detected in urban and agricultural regions using HH, VV and optimum

As PS pixels and SDFP pixels relate to different scattering characteristics of the ground, we also compared the density of measurements for both of the methods in urban and nonurban regions. Table I describes the percentage of additional pixels identified by SDFP pixels in comparison to PS pixels for which the results were previously published in [17]. For the HH and VV channels we detect about 8% more SDFP pixels than PS in agricultural regions, however, over the urban area the number of identified SDFPs is almost 9 percent less than PS pixels.

TABLE I
QUANTITATIVE COMPARISON OF IDENTIFIED SDFP PIXELS WITH RESPECT TO PS PIXELS (EXPRESSED IN PERCENT OF PS PIXELS)

Dataset	Agricultural	Urban
HH	8.5 %	-9.0 %
VV	8.2 %	-8.9 %
Optimum	10.3 %	-7.9 %

Similar to the HH and VV channels, in the case of the optimum channel, the small baseline method detects 10 percent more coherent pixels in agricultural regions, while in urban area the PS pixels are more numerous than SDFP pixels by about 8 percent. SDFP pixels show little loss of correlation in short time intervals whereas PS pixels remain stable over the whole period of data acquisition. Therefore, in non-urban area more SDFP pixels are expected to be identified than PS pixels. By contrast, in urban areas PS pixels are more abundant. This might be related to the effect of filtering in the small baseline method, which increases the decorrelation in pixels dominated by a single scatterer as a result of coarsening the resolution of spectra [13].

In order to check that using the optimum channel leads to lower phase noise, we selected SDFP pixels approximately every 0.001 degrees in both directions, and calculated the variance of the phase differences between the selected pixels and their immediate SDFP neighbors for the optimum, HH and VV channels. The results are plotted in Fig. 8.

The standard deviation of differences are very similar for HH and VV, but are generally lower for the optimum channel, indicating that our method leads to reduced phase noise. There appear to be two populations of pixels, however; those for which the improvement is marginal, and those for which the improvement is more significant (indicated in Fig 8a). This division is not apparently related to scattering mechanism, but does appear to correlate with spatial position (Fig. 9), with pixels in urban areas, plotted in red, more likely to fall in the population with greatest improvement.

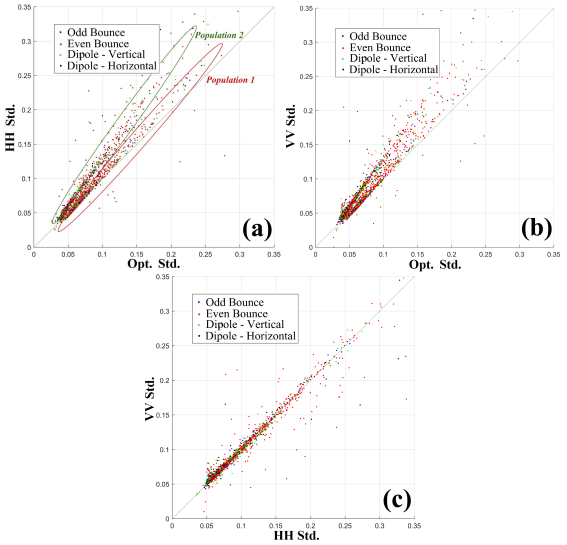

Fig. 8. Cross comparison of Standard deviation of phase differences of nearby SDFP pixels for the selected SDFP pixels for a) HH versus Optimum channel, the two populations marked by green and red eclipse are spatially located in fig. 9, b) VV versus optimum channel and c) HH versus VV channel . Blue and red dots indicate odd-bounce and even-bounce scattering mechanisms, respectively. Green and black colors indicate vertical and horizontal dipole scattering mechanism, respectively.

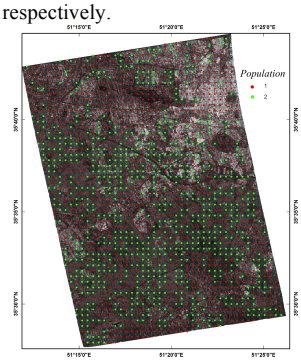

Fig. 9. Spatial position of the pixels in the two populations indicated in Fig 8a. Red circles depict the pixels located in the population where the reduction in standard deviation is most significant and the other population members are drawn in green.

Fig. 10 shows the time series for three sample SDFP pixels with odd-bounce (point 1), even-bounce (point 2) and dipole (point 3) scattering mechanisms, respectively, that were selected using the optimal channel, but not when using HH and VV channels. The smoothness of each of the time series indicates that the phase values have a low contribution from noise and that our algorithm is not increasing the number of selected pixels simply by selecting more noisy pixels.

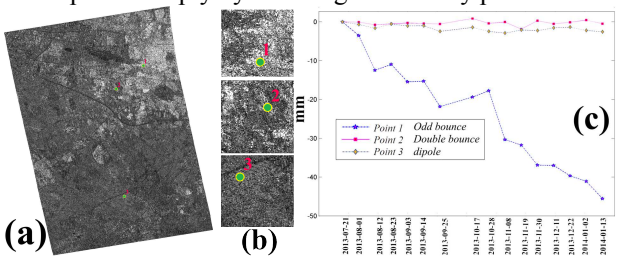

Fig. 10. a) location of the three points which detected by our method but not by using HH and VV. b) Closer look of he points in (a), point 1 is located in a farming zone and shows odd bounce mechanism, point 2 is located in an urban area with the dominant scattering mechanism for the pixel being double bounce and point 3 is a dipole. c) Time series plot of the selected points.

V. Conclusion

StaMPS is a powerful method for multi-temporal analysis of single channel SAR images [13]. In this paper, we have presented a small baseline method, implemented in StaMPS, to deal with dual polarization SAR images. The ADD index criterion is first minimized for dual polarimetric data to find the optimum scattering mechanism that lead to increase the number of SDFP candidates. Then the results are combined with temporal coherence criteria to select final coherent pixels for time-series analysis. Our experiment in both urban and agricultural regions, shows that applying our method for dual-pol data increased the number of SDFP pixels by 50% in comparison to single-pol data InSAR time-series analysis. In addition, the assessment between the result of our proposed method for small baseline algorithm with those from PS-InSAR polarimetric optimization [17], showed that the density of SDFP pixels, in small baseline approach, is more than PS pixels in non-urban regions, while, in urban area the number of PS pixels is slightly higher than the SDFP pixels. Future research could focus on implementing this type of polarimetric optimization on full/quad polarimetry SAR images. Also, joint optimization using the PSI approach [17], [22] and our new algorithm could improve the ability to find stable points for a large range of ground scattering characteristics.

Acknowledgment

Copyright of TerraSAR-X data belongs to German Aerospace Agency (DLR) and were provided by the project Motagh_XTI_LAND505.

References

[1] F. Amelung, D. L. Galloway, J. W. Bell, H. A. Zebker, and R. J. Laczniak, "Sensing the ups and downs of Las Vegas: InSAR reveals structural control of land subsidence and aquifer-system deformation," *Geology*, vol. 27, no. 6, pp. 483–486, 1999.

[2] G. Fornaro, A. Pauciullo, and F. Serafino, "Deformation monitoring over large areas with multipass differential SAR interferometry: a new approach based on the use of spatial differences," *Int. J. Remote Sens.*, vol. 30, no. 6, pp. 1455–1478, 2009.

[3] D. Massonnet *et al.*, "The displacement field of the Landers earthquake mapped by radar interferometry," *Nature*, vol. 364, no. 6433, pp. 138–142, Jul. 1993.

[4] M. Motagh *et al.*, "Subduction earthquake deformation associated with 14 November 2007, Mw 7.8 Tocopilla earthquake in Chile: Results from InSAR and aftershocks," *Tectonophysics*, vol. 490, no. 1–2, pp. 60–68, 2010.

[5] H. A. Zebker and J. Villasenor, "Decorrelation in interferometric radar echoes," *Geosci. Remote Sens. IEEE Trans. On*, vol. 30, no. 5, pp. 950–959, Sep. 1992.

[6] A. Ferretti, C. Prati, and F. Rocca, "Nonlinear subsidence rate estimation using permanent scatterers in differential SAR interferometry," *Geosci. Remote Sens. IEEE Trans. On*, vol. 38, no. 5, pp. 2202–2212, 2000.

[7] Ferretti, A., C. Prati, and F. Rocca, "Permanent scatterers in SAR interferometry," *IEEE Trans Geosci Remote Sens. 39 1 8 – 20*, 2001.

[8] A. Hooper, "A new method for measuring deformation on volcanoes and other natural terrains using InSAR persistent scatterers," *Geophys. Res. Lett.*, vol. 31, no. 23, 2004.

[9] P. Berardino, G. Fornaro, R. Lanari, and E. Sansosti, "A new algorithm for surface deformation monitoring based on small baseline differential SAR interferograms," *IEEE Trans. Geosci. Remote Sens.*, vol. 40, no. 11, pp. 2375–2383, Nov. 2002.

[10] O. Mora, J. J. Mallorqui, and A. Broquetas, "Linear and nonlinear terrain deformation maps from a reduced set of interferometric sar images," *IEEE Trans. Geosci. Remote Sens.*, vol. 41, no. 10, pp. 2243–2253, Oct. 2003.

[11] D. A. Schmidt and R. Bürgmann, "Time-dependent land uplift and subsidence in the Santa Clara valley, California, from a large interferometric synthetic aperture radar data set: SANTA CLARA VALLEY INSAR TIME SERIES," *J. Geophys. Res. Solid Earth*, vol. 108, no. B9, Sep. 2003.

[12] R. Lanari, O. Mora, M. Manunta, J. J. Mallorqui, P. Berardino, and E. Sansosti, "A small-baseline approach for investigating deformations on full-resolution differential SAR interferograms," *IEEE Trans. Geosci. Remote Sens.*, vol. 42, no. 7, pp. 1377–1386, Jul. 2004.

[13] A. Hooper, "A multi-temporal InSAR method incorporating both persistent scatterer and small baseline approaches," *Geophys. Res. Lett.*, vol. 35, no. 16, Aug. 2008.

[14] S. R. Cloude and K. P. Papathanassiou, "Polarimetric SAR interferometry," *Geosci. Remote Sens. IEEE Trans. On*, vol. 36, no. 5, pp. 1551–1565, 1998.

[15] E. Colin, C. Titin-Schnaider, and W. Tabbara, "An interferometric coherence optimization method in radar polarimetry for high-resolution imagery," *IEEE Trans. Geosci. Remote Sens.*, vol. 44, no. 1, pp. 167–175, Jan. 2006.

[16] P. Dheenathayalan and R. Hanssen, "Target characterization and interpretation of deformation using persistent scatterer interferometry and polarimetry," in *5th International Workshop on Science and Applications of SAR Polarimetry and Polarimetric Interferometry, 'POLInSAR 2011*, 2011.

[17] M. Esmaeili and M. Motagh, "Improved Persistent Scatterer analysis using Amplitude Dispersion Index optimization of dual polarimetry data," *ISPRS J. Photogramm. Remote Sens.*, vol. 117, pp. 108–114, Jul. 2016.

[18] S. Alipour, K. F. Tiampo, S. Samsonov, and P. J. Gonzalez, "Multibaseline PolInSAR Using RADARSAT-2 Quad-Pol Data: Improvements in Interferometric Phase Analysis," *IEEE Geosci. Remote Sens. Lett.*, vol. 10, no. 6, pp. 1280–1284, Nov. 2013.

[19] D. Monells, J. Mallorqui, G. Centolanza, and C. Lopez-Martinez, "Application of Polarimetric Techniques in DinSAR Processing for Space Borne Subsidence Monitoring," in *PolinSAR 2011, Science and Applications of SAR Polarimetry and Polarimetric Interferometry*, 2011, vol. 695, p. 22.

[20] L. Pipia *et al.*, "Polarimetric Differential SAR Interferometry: First Results With Ground-Based Measurements," *IEEE Geosci. Remote Sens. Lett.*, vol. 6, no. 1, pp. 167–171, Jan. 2009.

[21] V. D. Navarro-Sanchez and J. M. Lopez-Sanchez, "Subsidence monitoring using polarimetric persistent scatterers interferometry," in *Geoscience and Remote Sensing Symposium (IGARSS), 2011 IEEE International*, 2011, pp. 1083–1086.

[22] V. D. Navarro-Sanchez and J. M. Lopez-Sanchez, "Improvement of Persistent-Scatterer Interferometry Performance by Means of a Polarimetric Optimization," *IEEE Geosci. Remote Sens. Lett.*, vol. 9, no. 4, pp. 609–613, Jul. 2012.

[23] V. D. Navarro-Sanchez, J. M. Lopez-Sanchez, and L. Ferro-Famil, "Polarimetric Approaches for Persistent Scatterers Interferometry," *IEEE Trans. Geosci. Remote Sens.*, vol. 52, no. 3, pp. 1667–1676, Mar. 2014.

[24] S. Samsonov and K. Tiampo, "Polarization Phase Difference Analysis for Selection of Persistent Scatterers in SAR Interferometry," *IEEE Geosci. Remote Sens. Lett.*, vol. 8, no. 2, pp. 331–335, Mar. 2011.

[25] R. Iglesias, D. Monells, X. Fabregas, J. J. Mallorqui, A. Aguasca, and C. Lopez-Martinez, "Phase Quality Optimization in Polarimetric Differential SAR Interferometry," *IEEE Trans. Geosci. Remote Sens.*, pp. 1–14, 2013.

[26] B. Wu, T. Ling, Yan Chen, and H. Lei, "New Methods in Multibaseline Polarimetric SAR Interferometry Coherence Optimization," *IEEE Geosci. Remote Sens. Lett.*, vol. 12, no. 10, pp. 2016–2020, Oct. 2015.

[27] S. R. Cloude and K. P. Papathanassiou, "Polarimetric optimisation in radar interferometry," *Electron. Lett.*, vol. 33, no. 13, pp. 1176–1178, 1997.

[28] M. Neumann, L. Ferro-Famil, and A. Reigber, "Multibaseline polarimetric SAR interferometry coherence optimization," *Geosci. Remote Sens. Lett. IEEE*, vol. 5, no. 1, pp. 93–97, 2008.

[29] M. Motagh *et al.*, "Land subsidence in Iran caused by widespread water reservoir overexploitation," *Geophys. Res. Lett.*, vol. 35, no. 16, Aug. 2008.